JOURNAL OF GUIDANCE, CONTROL, AND DYNAMICS
Vol. 34, No. 4, July–August 2011

Optimal Rendezvous Trajectories of a Controlled Spacecraft and a Tumbling Object

George Boyarko,* Oleg Yakimenko,† and Marcello Romano‡
Naval Postgraduate School, Monterey, California 93943-5107

DOI: 10.2514/1.47645

This paper formulates and solves the problem of minimum-time and minimum-energy optimal trajectories of rendezvous of a powered chaser and a passive tumbling target, in a circular orbit. Both translational and rotational dynamics are considered. In particular, ending conditions are imposed of matching the positions and velocities of two points of interest onboard the vehicles. A collision-avoidance condition is imposed as well. The optimal control problems are analytically formulated through the use of the Pontryagin minimum principle. The problems are then solved numerically, by using a direct collocation method based on the Gauss pseudospectral approach. Finally, the obtained solutions are verified through the minimum principle, solved by a shooting method. The simulation results show that the pseudospectral solver provides solutions very close to the optimal ones, except in the case of presence of singular arcs when it may not provide a feasible solution. The computational time needed by the pseudospectral solver is a small fraction of the one needed by the indirect approach, but it is still considerably too large to allow for its use in real-time onboard guidance.

Nomenclature

d_i^C = position vector of the chaser docking point with respect to the chaser center of mass expressed in the chaser body frame ($i = x, y, z$)
d_i^T = position vector of the target docking point with respect to the target center of mass expressed in the target body frame ($i = x, y, z$)
m = mass of the chaser spacecraft
${}^O\omega_i^C$ = Cartesian components of the chaser spacecraft angular velocity of with respect to the orbital frame, expressed in the chaser spacecraft principal body coordinate frame ($i = x, y, z$)
${}^O\omega_i^T$ = Cartesian components of the target spacecraft angular velocity of with respect to the orbital frame, expressed in the target spacecraft principal body coordinate frame ($i = x, y, z$)
q_i^C = components of the quaternion, representing rotation from the orbital to chaser body frame ($i = 1, 2, 3, 4$)
q_i^T = components of the quaternion, representing rotation from the orbital to target body frame ($i = 1, 2, 3, 4$)
x, y, z = Cartesian coordinates of the chaser spacecraft center of mass in the Hill's coordinate frame
$\dot{x}, \dot{y}, \dot{z}$ = Cartesian components of the chaser spacecraft velocity in the Hill's coordinate frame
Ω = angular rate of the orbital frame with respect to the inertial frame
ω_i^C = Cartesian components of the chaser spacecraft angular velocity with respect to the inertial frame, expressed in the chaser spacecraft principal body coordinate frame ($i = x, y, z$)
ω_i^T = Cartesian components of the target spacecraft angular velocity with respect to the inertial frame, expressed in the target spacecraft principal body coordinate frame ($i = x, y, z$)

Presented as Paper 2009-5669 at the AIAA Guidance, Navigation, and Control Conference, Chicago, IL, 10–13 August 2009; received 16 October 2009; revision received 4 October 2010; accepted for publication 5 October 2010.

*Graduate Student, Department of Mechanical and Aerospace Engineering; gboyarko@nps.edu. Member AIAA.
†Research Professor, Department of Mechanical and Aerospace Engineering, Code MAE/Yk; oayakime@nps.edu. Associate Fellow AIAA.
‡Associate Professor, Department of Mechanical and Aerospace Engineering, Code MAE/MR; mromano@nps.edu. Associate Fellow AIAA.

I. Introduction

THE rendezvous problem of two spacecraft orbiting the Earth has been addressed in numerous publications. Rendezvous technology has also evolved with small-spacecraft development, such as the Demonstration for Autonomous Rendezvous Technology (DART),[§] the Experimental Satellite Systems-10 (XSS-10) and XSS-11[¶] [1], the Spacecraft for the Universal Modification of Orbits (SUMO) [2], and the Orbital Express (OE). In particular, the XSS-11 exhibited the ability for a small satellite to autonomously plan and rendezvous with a passive or cooperative resident space object (RSO) in low Earth orbit [3]. The use of microsatellites to inspect, service, repair, and refuel larger spacecraft is a long-term goal. The closest the XSS-11 approached and maneuvered around another object in space was approximately 500 m. In addition, DARPA's OE Advanced Technology Demonstration Program validated the technology and techniques for on-orbit refueling and reconfiguration of two satellites. The mission, conducted in 2007, performed several autonomous rendezvous and capture scenarios, including component exchange and propellant transfer events [4,5]. The existence of these programs demonstrates that there is a need for a robust and effective autonomous close-proximity control algorithm for multiple small spacecraft.

From the theoretical standpoint, the present paper elaborates on the previous work by Ma et al. [6], who have studied the minimum-control-effort problem for a planar rendezvous to a tumbling object (with only three states, position coordinates x and y, and heading angle θ), neglecting any path constraints and relative motion dynamics pertinent to proximity space operations. The Sakawa–Shindo algorithm [7] was used for calculating the optimal control. The current paper greatly expands the scope by taking into account the proximity motion dynamics, considering the full six-degree-of-freedom model and determining both the minimum-time and the minimum-control (energy) effort solution of the rendezvous of two satellites. It also features a comparison of the solutions obtained

[§]NASA, DART Mission, http://www.nasa.gov/missions/science/dart_into_space.html [retrieved 20 July 2009].
[¶]U.S. Air Force Research Laboratory, XSS-11, http://www.kirtland.af.mil/shared/media/document/AFD-070404-108.pdf [retrieved 20 July 2009].

using one of the prominent direct methods with the truly optimal solutions obtained using the minimum principle (MP). Another paper by the authors takes a further step and considers three different performance indexes adding additional constraints to match terminal attitude and angular rate, along with position and velocity [8].

This paper is organized as follows. Section II introduces the dynamics model of two spacecraft and formulates the optimal control problem. Section III synthesizes the optimal solution by exploiting the minimum principle. Section IV presents a methodology of solving optimal control problems using one of the pseudospectral methods (PSM) and verifying the solution converting the optimal control problem to a two-point boundary-value problem (TPBVP), i.e., a problem of minimization of a scalar function of several variables, and solving it via a forward-shooting technique using a quasi-Newton method. Next, Sec. V presents the results using the developed methodology to solve the minimum-control (energy) problem, followed by Sec. VI that addresses the minimum-time problem.

II. Two-Spacecraft Rendezvous Modeling and Optimization Problem Formulation

This section develops a model of target-chaser rendezvous. Figures 1 and 2 show a graphical representation of the problem. The center of the orbit frame is fixed to the center of mass of the tumbling RSO. The x axis points toward the zenith. The y axis lies along the velocity vector of the RSO (assuming circular orbit) and the z axis lies along the orbit normal of the RSO. We start from the arbitrary relative position (Fig. 1a) and would like to bring two spacecraft together for docking (Fig. 1b).

Using the notations described in the beginning of this paper based on the above model, the dynamics of the two systems can now be described as follows. The translational kinematics and dynamics of a chaser spacecraft in the orbit frame centered at the target vehicle are given by the Hill–Clohessy–Wiltshire equations [9]:

$$\begin{aligned}\ddot{x} &= \frac{1}{m}(2\Omega\dot{y} + 3\Omega^2 x + f_x)\\ \ddot{y} &= \frac{1}{m}(-2\Omega\dot{x} + f_y)\\ \ddot{z} &= \frac{1}{m}(-\Omega^2 z + f_z)\end{aligned} \tag{1}$$

where f_x, f_y, and f_z are the applied forces (controls) expressed in the Hill frame.

The rotational dynamics of the chaser, described by the vector equation [10,11]

$$\mathbf{I}^C\dot{\boldsymbol{\omega}}^C + \boldsymbol{\omega}^C \times \mathbf{I}^C\boldsymbol{\omega}^C = \mathbf{T} \tag{2}$$

expand into the scalar quantities

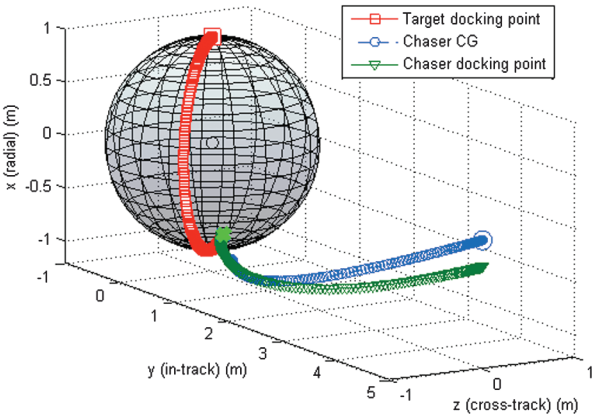

Fig. 2 Three-dimensional view of the minimum-control trajectory given by the pseudospectral solver.

$$\begin{aligned}\dot{\omega}_z^C &= \frac{(I_{22}^C - I_{33}^C)\omega_y^C\omega_z^C + T_x^C}{I_{11}^C}, \qquad \dot{\omega}_y^C = \frac{(I_{33}^C - I_{11}^C)\omega_x^C\omega_z^C + T_y^C}{I_{22}^C}\\ \dot{\omega}_z^C &= \frac{(I_{11}^C - I_{22}^C)\omega_y^C\omega_x^C + T_z^C}{I_{33}^C}\end{aligned} \tag{3}$$

In Eqs. (2) and (3), $\mathbf{I}^C = \mathrm{diag}([I_{11}^C, I_{22}^C, I_{33}^C])$ is the inertia matrix along the principal axes, $\boldsymbol{\omega}^C = [\omega_x^C, \omega_y^C, \omega_z^C]^T$, and $\mathbf{T} = [T_x, T_y, T_z]^T$ is the torque vector (superscript T denotes transposition).

Similarly, for the (uncontrolled) target the rotational dynamics are given by the vector equation

$$\mathbf{I}^T\dot{\boldsymbol{\omega}}^T + \boldsymbol{\omega}^T \times \mathbf{I}^T\boldsymbol{\omega}^T = \mathbf{0} \tag{4}$$

or in scalar form,

$$\begin{aligned}\dot{\omega}_x^T &= -\frac{(I_{33}^T - I_{22}^T)\omega_y^T\omega_z^T}{I_{11}^T}, \qquad \dot{\omega}_y^T = -\frac{(I_{11}^T - I_{33}^T)\omega_x^T\omega_z^T}{I_{22}^T},\\ \dot{\omega}_z^T &= -\frac{(I_{22}^T - I_{11}^T)\omega_y^T\omega_x^T}{I_{33}^T}\end{aligned} \tag{5}$$

Defining ${}_T^O\mathbf{R}$ as the rotation matrix to convert from the body frame of the target $\{T\}$ to the orbital frame $\{O\}$ and ${}_C^O\mathbf{R}$ to convert from the chaser body frame $\{C\}$ to the orbital frame $\{O\}$, we can define the angular velocity of each object ($\alpha = \{T, C\}$) with respect to the orbital frame expressed in the orbital frame:

$$\begin{bmatrix} {}^O\omega_x^\alpha \\ {}^O\omega_y^\alpha \\ {}^O\omega_z^\alpha \end{bmatrix} = {}_\alpha^O\mathbf{R}\begin{bmatrix} \omega_x^\alpha \\ \omega_y^\alpha \\ \omega_z^\alpha \end{bmatrix} - \begin{bmatrix} 0 \\ 0 \\ \Omega \end{bmatrix} \tag{6}$$

Rotation matrices ${}_\alpha^O\mathbf{R}$ are constructed using components of the corresponding quaternion as follows [10]:

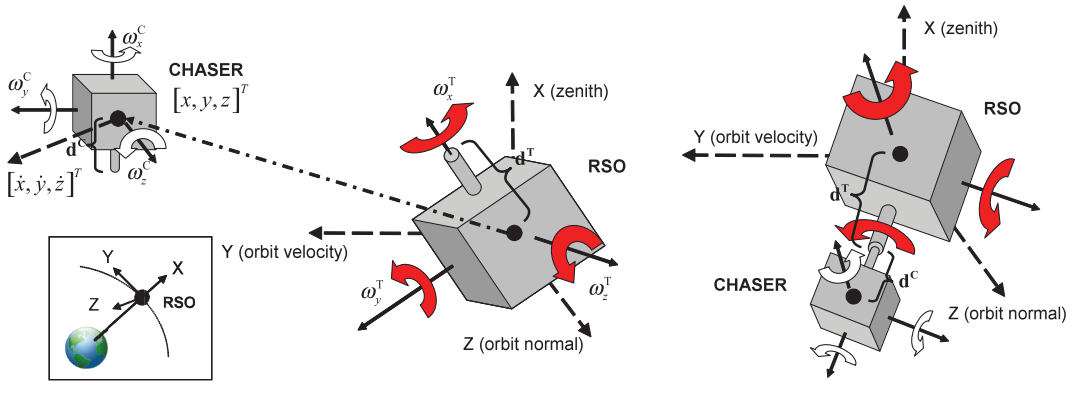

Fig. 1 Depiction of the a) two-spacecraft rendezvous problem and b) desired final state at t_f.

$$
{}^{O}_{\alpha}\mathbf{R} = \begin{bmatrix} q_4^{\alpha 2} + q_1^{\alpha 2} - q_2^{\alpha 2} - q_3^{\alpha 2} & 2(q_1^\alpha q_2^\alpha - q_3^\alpha q_4^\alpha) & 2(q_1^\alpha q_3^\alpha + q_2^\alpha q_4^\alpha) \\ 2(q_1^\alpha q_2^\alpha + q_3^\alpha q_4^\alpha) & q_4^{\alpha 2} - q_1^{\alpha 2} + q_2^{\alpha 2} - q_3^{\alpha 2} & 2(q_2^\alpha q_3^\alpha - q_1^\alpha q_4^\alpha) \\ 2(q_1^\alpha q_3^\alpha - q_2^\alpha q_4^\alpha) & 2(q_2^\alpha q_3^\alpha + q_1^\alpha q_4^\alpha) & q_4^{\alpha 2} - q_1^{\alpha 2} - q_2^{\alpha 2} + q_3^{\alpha 2} \end{bmatrix} \tag{7}
$$

The elements of the quaternion are propagated according to [10]

$$
\begin{bmatrix} \dot{q}_1^\alpha \\ \dot{q}_2^\alpha \\ \dot{q}_3^\alpha \\ \dot{q}_4^\alpha \end{bmatrix} = \frac{1}{2} \begin{bmatrix} 0 & {}^{O}\omega_z^\alpha & -{}^{O}\omega_y^\alpha & {}^{O}\omega_x^\alpha \\ -{}^{O}\omega_z^\alpha & 0 & {}^{O}\omega_x^\alpha & {}^{O}\omega_y^\alpha \\ {}^{O}\omega_y^\alpha & -{}^{O}\omega_x^\alpha & 0 & {}^{O}\omega_z^\alpha \\ -{}^{O}\omega_x^\alpha & -{}^{O}\omega_y^\alpha & -{}^{O}\omega_z^\alpha & 0 \end{bmatrix} \begin{bmatrix} q_1^\alpha \\ q_2^\alpha \\ q_3^\alpha \\ q_4^\alpha \end{bmatrix} \tag{8}
$$

Equations (1), (3), (5), and (8), define a 20-state system of differential equations governing rendezvous dynamics. Combined into the state vector $\mathbf{x}$ these states are

$$
\begin{aligned} \mathbf{x} = [&x, y, z, \dot{x}, \dot{y}, \dot{z}, \omega_x^C, \omega_y^C, \omega_z^C, \omega_x^T, \omega_y^T, \omega_z^T, \\ &q_1^C, q_2^C, q_3^C, q_4^C, q_1^T, q_2^T, q_3^T, q_4^T]^T \end{aligned} \tag{9}
$$

The governing dynamics assume six normalized controls that can be used by the chaser to achieve the rendezvous conditions:

$$
\mathbf{u} = \left[\frac{f_x}{f_{x\max}}, \frac{f_y}{f_{y\max}}, \frac{f_z}{f_{z\max}}, \frac{T_x}{T_{x\max}}, \frac{T_y}{T_{y\max}}, \frac{T_z}{T_{z\max}} \right]^T \tag{10}
$$

For simplicity, we will further assume that $f_{i\max} = 1$ ms^{-2} and $T_{i\max} = 1$ Nm for $i = x, y, z$, Once again, these controls are three normalized components of a translational force acting on a chaser f_i $(i = x, y, z)$, expressed in the Hill coordinate frame, and three normalized components of a torque allowing change in the chaser's attitude, T_i $(i = x, y, z)$, expressed in the chaser's body frame. All six controls are bounded: $-\mathbf{1} \le \mathbf{u} \le \mathbf{1}$.

Using these controls we would like to bring the two spacecraft from some initial conditions, given by 20 initial values of states $x_i(t_0)$, $i = 1, \ldots, 20$, to docking-enabling conditions described by matching the chaser's and target's docking-station final positions and velocity vectors. These docking-enabling conditions can be conveniently expressed by the following six end conditions, depending on the state variables:

$$
\begin{aligned} &{}^{O}_{T}\mathbf{R} \begin{bmatrix} d_x^T \\ d_y^T \\ d_z^T \end{bmatrix} - \left({}^{O}_{C}\mathbf{R} \begin{bmatrix} d_x^C \\ d_y^C \\ d_z^C \end{bmatrix} + \begin{bmatrix} x \\ y \\ z \end{bmatrix} \right) = \begin{bmatrix} e_1 \\ e_2 \\ e_3 \end{bmatrix} = \mathbf{0} \text{ and} \\ &{}^{O}\boldsymbol{\omega}^T \times {}^{O}_{T}\mathbf{R} \begin{bmatrix} d_x^T \\ d_y^T \\ d_z^T \end{bmatrix} - \left({}^{O}\boldsymbol{\omega}^C \times {}^{O}_{C}\mathbf{R} \begin{bmatrix} d_x^C \\ d_y^C \\ d_z^C \end{bmatrix} + \begin{bmatrix} \dot{x} \\ \dot{y} \\ \dot{z} \end{bmatrix} \right) = \begin{bmatrix} e_4 \\ e_5 \\ e_6 \end{bmatrix} = \mathbf{0} \end{aligned} \tag{11}
$$

While transitioning to docking-enabling conditions we would like to minimize and compare two different performance indices,

$$
J = \int_{t_0}^{t_f} f_0 \, \mathrm{d}t \tag{12}
$$

with

$$
f_0 = 1 \tag{13}
$$

for minimum time and

$$
f_0 = \tfrac{1}{2}(u_1^2 + u_2^2 + u_3^2 + u_4^2 + u_5^2 + u_6^2) \tag{14}
$$

for minimum quadratic control (or energy) expenditure.

III. Synthesis of the Optimal Control Using the Minimum Principle

This section deals with the MP and synthesis of the optimal control in order to analyze its structure and reduce the problem to a TPBVP.

A. Formulation of the Optimal Control Problem

We start from the general formulation for the Hamiltonian of the system with the state vector $\mathbf{x}$, Eq. (9), control vector $\mathbf{u}$, Eq. (10), and running cost f_0:

$$
H(\boldsymbol{\lambda}, \mathbf{x}, \mathbf{u}) := f_0 + (\boldsymbol{\lambda}, \dot{\mathbf{x}}) \tag{15}
$$

where the operator $(\ldots)$ denotes a scalar product of two vectors, and $\boldsymbol{\lambda} \in \Re^{N_x}$ is a costate vector whose differential equations are to be defined later in this section.

For the specific system of equations (1), (3), (5), and (8), with the running cost from Eq. (13) (minimum-time problem) the Hamiltonian can be written as

$$
\begin{aligned} H(\boldsymbol{\lambda}, \mathbf{x}, \mathbf{u}) := {} & +\lambda_1 x_4 + \lambda_2 x_5 + \lambda_3 x_6 + \frac{1}{m}(\lambda_4(2\Omega x_5 + 3\Omega^2 x_1 \\ & + u_1) + \lambda_5(-2\Omega x_4 + u_2) + \lambda_6(-\Omega^2 x_3 + u_3)) \\ & + \frac{(I_{22}^C - I_{33}^C)x_8 x_9 + u_4}{I_{11}^C}\lambda_7 + \frac{(I_{33}^C - I_{11}^C)x_7 x_9 + u_5}{I_{22}^C}\lambda_8 \\ & + \frac{(I_{11}^C - I_{22}^C)x_8 x_7 + u_6}{I_{33}^C}\lambda_9 + \frac{(I_{22}^T - I_{33}^T)x_{11} x_{12}}{I_{11}^T}\lambda_{10} \\ & + \frac{(I_{33}^T - I_{11}^T)x_{10} x_{12}}{I_{22}^T}\lambda_{11} + \frac{(I_{11}^T - I_{22}^T)x_{11} x_{10}}{I_{33}^T}\lambda_{12} + \lambda_{13}\frac{1}{2}((x_9 \\ & - (x_{16}^2 - x_{13}^2 - x_{14}^2 + x_{15}^2)\Omega)x_{14} - (x_8 - 2(x_{14}x_{15} \\ & - x_{13}x_{16})\Omega)x_{15} + (x_7 - 2(x_{13}x_{15} + x_{14}x_{16})\Omega)x_{16}) \\ & + \lambda_{14}\frac{1}{2}(-(x_9 - (x_{16}^2 - x_{13}^2 - x_{14}^2 + x_{15}^2)\Omega)x_{13} + (x_8 \\ & - 2(x_{14}x_{15} - x_{13}x_{16})\Omega)x_{16} + (x_7 - 2(x_{13}x_{15} \\ & + x_{14}x_{16})\Omega)x_{15}) + \lambda_{15}\frac{1}{2}(-(x_7 - 2(x_{13}x_{15} + x_{14}x_{16})\Omega)x_{14} \\ & + (x_8 - 2(x_{14}x_{15} - x_{13}x_{16})\Omega)x_{13} + (x_9 - (x_{16}^2 - x_{13}^2 - x_{14}^2 \\ & + x_{15}^2)\Omega)x_{16}) + \lambda_{16}\frac{1}{2}(-(x_7 - 2(x_{13}x_{15} + x_{14}x_{16})\Omega)x_{13} \\ & - (x_8 - 2(x_{14}x_{15} - x_{13}x_{16})\Omega)x_{14} - (x_9 - (x_{16}^2 - x_{13}^2 - x_{14}^2 \\ & + x_{15}^2)\Omega)x_{15}) + \lambda_{17}\frac{1}{2}((x_{12} - (x_{20}^2 - x_{17}^2 - x_{18}^2 + x_{19}^2)\Omega)x_{18} \\ & - (x_{11} - 2(x_{18}x_{19} - x_{17}x_{20})\Omega)x_{19} + (x_{10} - 2(x_{17}x_{19} \\ & + x_{18}x_{20})\Omega)x_{20}) + \lambda_{18}\frac{1}{2}(-(x_{12} - (x_{20}^2 - x_{17}^2 - x_{18}^2 \\ & + x_{19}^2)\Omega)x_{17} + (x_{11} - 2(x_{18}x_{19} - x_{17}x_{20})\Omega)x_{20} + (x_{10} \\ & - 2(x_{17}x_{19} + x_{18}x_{20})\Omega)x_{19}) + \lambda_{19}\frac{1}{2}(-(x_{10} - 2(x_{17}x_{19} \\ & + x_{18}x_{20})\Omega)x_{18} + (x_{11} - 2(x_{18}x_{19} - x_{17}x_{20})\Omega)x_{17} + (x_{12} \\ & - (x_{20}^2 - x_{17}^2 - x_{18}^2 + x_{19}^2)\Omega)x_{20}) + \lambda_{20}\frac{1}{2}(-(x_{10} - 2(x_{17}x_{19} \\ & + x_{18}x_{20})\Omega)x_{17} - (x_{11} - 2(x_{18}x_{19} - x_{17}x_{20})\Omega)x_{18} - (x_{12} \\ & - (x_{20}^2 - x_{17}^2 - x_{18}^2 + x_{19}^2)\Omega)x_{19}) \end{aligned} \tag{16}
$$

The part of the Hamiltonian that depends on the controls, the switching function, for the time-minimum problem is

$$
\begin{aligned} H^*(\boldsymbol{\lambda}, \mathbf{x}, \mathbf{u}) = {} & \frac{1}{m}(\lambda_4 u_1 + \lambda_5 u_2 + \lambda_6 u_3) + \frac{1}{I_{11}^C}\lambda_7 u_4 \\ & + \frac{1}{I_{22}^C}\lambda_8 u_5 + \frac{1}{I_{33}^C}\lambda_9 u_6 \end{aligned} \tag{17}
$$

As shown, all six controls enter the switching function (Hamiltonian) linearly, and therefore the optimal control for all of them is the bang–bang control defined by

$$u_i = \begin{cases} 1, & \text{when } \lambda_{i+3} < 0 \\ -1, & \text{when } \lambda_{i+3} \geq 0 \end{cases} \quad \text{for } i = 1, \ldots, 6 \tag{18}$$

(the possibility of a singular control, when $\lambda_{i+3}(t) \equiv 0$, is considered in Sec. III.C).

Likewise, developing the Hamiltonian for the minimum-quadratic-control cost function, or minimum energy, based on Eq. (14) the part of the Hamiltonian that depends on the controls is

$$H^*(\boldsymbol{\lambda}, \mathbf{x}, \mathbf{u}) := \frac{1}{2}(u_1^2 + u_2^2 + u_3^2 + u_4^2 + u_5^2 + u_6^2) + \frac{1}{m}(\lambda_4 u_1 + \lambda_5 u_2 + \lambda_6 u_3) + \frac{1}{I_{11}^C}\lambda_7 u_4 + \frac{1}{I_{22}^C}\lambda_8 u_5 + \frac{1}{I_{33}^C}\lambda_9 u_6 \tag{19}$$

Since the controls enter the Hamiltonian nonlinearly the optimal control is not a bang–bang anymore. To be more specific, the resulting optimal control that minimizes the Hamiltonian for the minimum-quadratic-control cost function Eq. (14) (minimum energy) is as follows:

$$u_i = \begin{cases} 1, & \frac{\lambda_{i+3}}{m} < -1 \\ \frac{\lambda_{i+3}}{m}, & -1 \frac{\lambda_{i+3}}{m} < 1 \\ -1, & \frac{\lambda_{i+3}}{m} \geq 1 \end{cases} \quad \text{for } i = 1, 2, 3,$$

$$u_i = \begin{cases} 1, & \frac{\lambda_{i+3}}{I_{kk}^C} < -1 \\ \frac{\lambda_{i+3}}{I_{kk}^C}, & -1 \frac{\lambda_{i+3}}{I_{kk}^C} < 1 \\ -1, & \frac{\lambda_{i+3}}{I_{kk}^C} \geq 1 \end{cases} \quad \text{for } i = 4, 5, 6, \quad \text{where } k = i - 3 \tag{20}$$

Now the differential equations for costates will be the same for both optimization problems and are obtained via

$$\dot{\boldsymbol{\lambda}} = -\left(\frac{\partial H}{\partial \mathbf{x}}\right)^T \tag{21}$$

For instance, the first six adjoint equations are given by

$$\dot{\lambda}_1 = -3\lambda_4 \Omega^2 m^{-1}, \qquad \dot{\lambda}_2 = 0, \qquad \dot{\lambda}_3 = \lambda_6 \Omega^2 m^{-1}$$
$$\dot{\lambda}_4 = -\lambda_1 + 2\lambda_5 \Omega m^{-1}, \qquad \dot{\lambda}_5 = -\lambda_2 - 2\lambda_4 \Omega m^{-1}$$
$$\dot{\lambda}_6 = -\lambda_3 \tag{22}$$

The next six adjoint equations, corresponding to the states 7 through 12, take the form of

$$\dot{\lambda}_7 = \frac{I_{11}^C - I_{33}^C}{I_{22}^C}\lambda_8 x_9 + \frac{I_{22}^C - I_{11}^C}{I_{33}^C}\lambda_9 x_8 - \lambda_{13}\frac{1}{2}\Omega x_{16} - \lambda_{14}\frac{1}{2}\Omega x_{15} + \lambda_{15}\frac{1}{2}\Omega x_{14} + \lambda_{16}\frac{1}{2}\Omega x_{13} \tag{23}$$

The remaining eight adjoint equations, corresponding to the states 13 through 20, are of the form

$$\begin{aligned} \dot{\lambda}_{13} = {} & -\lambda_{13}\frac{1}{2}(2x_{13}\Omega x_{14} - 2x_{16}\Omega x_{15} - 2x_{15}\Omega x_{16}) - \lambda_{14}\frac{1}{2}(-(x_9 \\ & - (x_{16}^2 - x_{13}^2 - x_{14}^2 + x_{15}^2)\Omega) - 2x_{13}^2\Omega - 2x_{16}^2\Omega - 2x_{15}^2\Omega) \\ & - \lambda_{15}\frac{1}{2}(2x_{15}\Omega x_{14} + (x_8 - 2(x_{14}x_{15} - x_{13}x_{16})\Omega) + 2x_{16}\Omega x_{13} \\ & + 2x_{13}\Omega x_{16}) - \lambda_{16}\frac{1}{2}(2x_{15}\Omega x_{13} - (x_7 - 2(x_{13}x_{15} \\ & + x_{14}x_{16})\Omega) - 2x_{16}\Omega x_{14} - 2x_{13}\Omega x_{15}) \end{aligned} \tag{24}$$

(The adjoint equations for $\lambda_{14}, \ldots, \lambda_{20}$ can be written by cyclic permutations of either the chaser or RSO state variables.)

Note that for this problem formulation, the third and the sixth costates are decoupled. This feature will be addressed further.

The transversality (end) conditions, which are additional necessary conditions for optimality, follow directly from Eq. (11) [12]:

$$\boldsymbol{\lambda}_{t_f} = -\upsilon_1 \left.\frac{\partial e_1}{\partial \mathbf{x}}\right|_{\mathbf{x}(t_f)} - \ldots - \upsilon_6 \left.\frac{\partial e_6}{\partial \mathbf{x}}\right|_{\mathbf{x}(t_f)} \tag{25}$$

where υ_i are additional parameters [12].

The first six equations in Eq. (25) result in expressions that contain only the parameters υ_i $(i = 1, \ldots, 6)$:

$$\lambda_1(t_f) = -\upsilon_1, \qquad \lambda_2(t_f) = -\upsilon_2, \qquad \lambda_3(t_f) = -\upsilon_3$$
$$\lambda_4(t_f) = -\upsilon_4, \qquad \lambda_5(t_f) = -\upsilon_5, \qquad \lambda_6(t_f) = -\upsilon_6 \tag{26}$$

These six equations are then properly substituted into the remaining 14 equations in Eq. (25). For example, for the seventh costate, the transversality condition becomes

$$\begin{aligned} \lambda_7(t_f) = {} & (2(x_{13}x_{14} + x_{15}x_{16})x_{23} - 2(x_{13}x_{15} - x_{14}x_{16})x_{22})|_{t_f}\upsilon_4 \\ & + (2(x_{13}x_{15} - x_{14}x_{16})x_{21} - (x_{16}^2 + x_{13}^2 - x_{14}^2 - x_{15}^2)x_{23})|_{t_f}\upsilon_5 \\ & + ((x_{16}^2 + x_{13}^2 - x_{14}^2 - x_{15}^2)x_{22} - 2(x_{13}x_{14} + x_{15}x_{16})x_{21})|_{t_f}\upsilon_6 \end{aligned} \tag{27}$$

Hence, in addition to $\mathbf{e}(t_f) = \mathbf{0}$ [Eq. (11)], the transversality conditions give the following 14 additional equalities to be satisfied at the terminal point:

$$\boldsymbol{\zeta}_{i-6}(t_f) = \lambda_i(t_f) - f_i(\mathbf{x}(t_f), \boldsymbol{\upsilon}) = 0 \qquad i = 7, \ldots, 20 \tag{28}$$

Finally, since the Hamiltonian is time-independent [12],

$$H(t_f) = 0 \tag{29}$$

Equations (11), (28), and (29), provide us with 21 terminal conditions to satisfy, which matches the number of varied parameters: the values of the initial costates $\lambda_i(t_0)$ $(i = 1, \ldots, 20)$ and the maneuver time t_f.

Finally, everything is ready to numerically solve the minimum-time problem converted to a nonlinear programming TPBVP problem. Specifically, given the 20 initial conditions on the states, given the 20 differential equations [Eqs. (1), (3), (5), and (8)] describing the system dynamics, the 20 differential equations describing the adjoint dynamics [Eqs. (22–24)], and the 21 terminal conditions [Eqs. (21), (28), and (29)], the optimal controls are synthesized as Eq. (18) or Eq. (20).

The problem is solved numerically, with a shooting approach, by forward integrating the 40 differential equations, forced by the synthesized optimal controls, for t_f seconds and checking the terminal conditions. If the conditions are not satisfied (within numerical tolerance), the values of the initial costates [$\lambda_i(t_0)$ for $i = 1, \ldots, 20$] and the final time t_f are appropriately changed, and the integration is repeated.

B. Collision Avoidance Through a Path Constraint

For the close-proximity rendezvous problem, a critical issue is the collision avoidance. The collision avoidance can be taken into consideration by imposing the following path constraint: the center of mass of the chaser spacecraft must remain at a distance larger than some minimum distance (a "keep-out" sphere with a radius r) from the center of mass of the RSO. This ensures that the chaser vehicle will not pass through the target vehicle in order to reach the docking position. Mathematically speaking, this can be defined as

$$h = (x_1^2 + x_2^2 + x_3^2) - r^2 \geq 0 \tag{30}$$

where x_i $(i = 1, 2, 3)$ are the first three elements of the state vector (9). Furthermore, while a trajectory is on a path constraint $h = 0$, the tangential condition must also be satisfied [13]:

$$\dot{h} = \frac{\mathrm{d}h}{\mathrm{d}t} = x_1 x_4 + x_2 x_5 + x_3 x_6 = 0 \tag{31}$$

Consequently, the Hamiltonian should be augmented by another term:

$$H(\boldsymbol{\lambda}, \mathbf{x}, \mathbf{u}) := f_0 + (\boldsymbol{\lambda}, \dot{\mathbf{x}}) + \mu \ddot{h} \tag{32}$$

where μ is a constant and

$$\ddot{h} = \frac{\mathrm{d}^2 h}{\mathrm{d}t^2} \tag{33}$$

(since the path constraint has to be differentiated with respect to time twice before the control variables appear in the expression). The value of μ is dictated as follows.

Off the constraint boundary,

$$\mu = 0 \quad \text{if } h > 0 \tag{34a}$$

On the constraint boundary,

$$\mu \geq 0 \quad \text{if } h = \dot{h} = \ddot{h} = 0 \tag{34b}$$

Therefore, upon first contact with the path constraint, the costate values and Hamiltonian will be discontinuous [13].

C. Possibility of a Singular Control for a Minimum-Time Problem

Upon closer inspection, we find that in the z direction the translational control u_3 is decoupled from all other controls. In particular, from Eq. (1) it is

$$\dot{x}_3 = x_6, \qquad \dot{x}_6 = m^{-1}(-\Omega^2 x_3 + u_3) \tag{35}$$

or

$$\ddot{x}_3 + m^{-1}\Omega^2 x_3 = m^{-1} u_3 \tag{36}$$

and Eq. (22) yields

$$\dot{\lambda}_3 = m^{-1}\Omega^2 \lambda_6, \qquad \dot{\lambda}_6 = -\lambda_3 \tag{37}$$

or

$$\ddot{\lambda}_6 + m^{-1}\Omega^2 \lambda_6 = 0 \tag{38}$$

For the minimum-time problem, the optimal control is defined as in Eq. (18); hence, for u_3 we will have

$$u_3 = \begin{cases} 1, & \lambda_6 < 0 \\ -1, & \lambda_6 > 0 \end{cases} \tag{39}$$

Taking into account Eq. (39), we can state that

$$u_3(t) = f(\lambda_3(t_0), \lambda_6(t_0)) \tag{40}$$

Defined by the natural frequency of Eq. (38) the control u_3 can switch from $u_{3\max} = 1$ to $u_{3\min} = -1$ or vice versa every $\pi\sqrt{m}\Omega^{-1}$ seconds. Moreover, the solution to Eq. (38) with the initial conditions defined by $\lambda_6(t_0)$ and $\dot{\lambda}_6(t_0) = -\lambda_3(t_0)$ can be found analytically:

$$\lambda_6(t) = -\lambda_3(t_0) m^{0.5}\Omega^{-1} \sin(m^{-0.5}\Omega t) + \lambda_6(t_0)\cos(m^{-0.5}\Omega t) \tag{41}$$

The roots of this equation are defined at

$$t = \tan^{-1}\left(\frac{\lambda_6(t_0)}{\lambda_3(t_0)} m^{-0.5}\Omega\right) m^{0.5}\Omega^{-1} \tag{42}$$

On the other hand, the extrema of Eq. (41) are achieved at

$$t^* = -\tan^{-1}\left(\frac{\lambda_3(t_0)}{\lambda_6(t_0)} m^{0.5}\Omega^{-1}\right) m^{0.5}\Omega^{-1} \tag{43}$$

As shown in Eqs. (41–43) the only possibility for singular control would be when

$$\lambda_3(t_0) = 0 \quad \text{and} \quad \lambda_6(t_0) = 0 \tag{44}$$

In this case $\lambda_6(t) = 0$ and the optimal control cannot be defined from Eq. (39), but requires more rigorous analysis [13].

IV. Methodology for Obtaining a Solution and Checking Its Optimality

This section presents the methodology for obtaining and verifying optimal solutions for the two problems posed in Sec. II. Despite the fact that the structure of an optimal control was defined analytically (in the previous section) it would be very difficult to solve this problem using a direct shooting approach with arbitrary initial values of the varied parameters, as the numerical solution would likely diverge. That is where direct methods of calculus of variations become useful. In what follows we first introduce a specific rendezvous scenario with the particular numerical values examined. Next, we describe a procedure for obtaining a quasi-optimal numerical solution for each of the two optimization problems using one of the direct collocation (pseudospectral) methods. Finally, a methodology of using this solution, which is very close to the true optimal one, to address the problem using a direct shooting method for the TPBVP formulated in Sec. III is introduced.

A. Defining Rendezvous Scenario

A sample maneuvering scenario is considered with the chaser center of mass starting at a distance of 5 m from the target center of mass, and with the target having an initial angular velocity of 0.25 rad/s in both y and z body axes. The body coordinate frames of each spacecraft and the orbit frame are assumed to be coincident with the inertial frame at the beginning of the simulation. The chaser docking point is located at $[-0.25, \quad 0, \quad 0]^T$ m in the body frame while the target docking point is located $[1, \quad 0, \quad 0]^T$ m in the target body frame. The initial values mentioned and the remaining states for computer simulations discussed in the following sections are presented in Table 1. Without loss of generality it is assumed that $m = 1$ kg, $\Omega = 0.005$ rad/s, $\mathbf{I}^C = \mathbf{I}^T = \mathbf{I}_{3\times3}$ (where $\mathbf{I}_{3\times3}$ is the identity matrix), $r^2 = 1.5$ m^2, and the maximum final time is 10 s.

B. Solving the Optimal Control Problems Using the Gauss Pseudospectral Optimization Solver

The optimal control problems posted in Secs. II were first solved using the Gauss Pseudospectral Optimization Solver (GPOPS) [14]. This is an open-source and freely available software package for solving optimal control problems. As many as 150 internal nodes were chosen for the solution (usually, to speed up the numerical procedure not more than about 60 nodes are used [15]). The initial

Table 1 Initial values of the states

State	Initial condition, m and m/s	State	Initial condition, rad/s	State	Initial condition (quaternion)	State	Initial condition (quaternion)
x_1	0	x_7	0	x_{13}	0	x_{17}	0
x_2	5	x_8	0	x_{14}	0	x_{18}	0
x_3	0	x_9	0	x_{15}	0	x_{19}	0
x_4	0	x_{10}	0	x_{16}	1	x_{20}	1
x_5	0	x_{11}	0.25	——	——	——	——
x_6	0	x_{12}	0.25	——	——	——	——

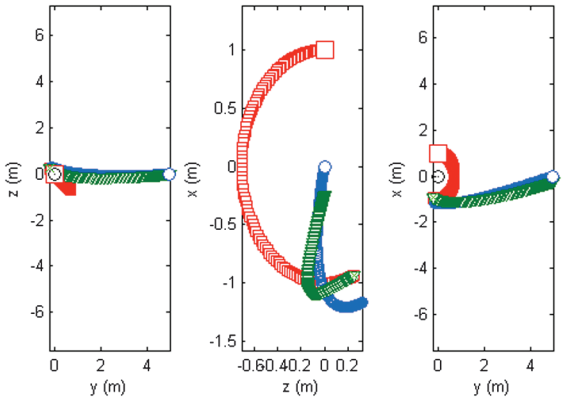

Fig. 3 Planar views of the minimum-control trajectory given by the pseudospectral solver.

conditions were chosen based on Table 1 and the final conditions were based on matching position and velocity of the terminal point (see Eq. (11)).

C. Verifying the Pseudospectral Solution with the Minimum Principle

The differential equations for the states [Eqs. (1), (3), (5), and (8)] and costates [Eqs. (21–24)], developed in the previous sections, were programmed into a MathWorks' Simulink model. This model is called from a MATLAB script by the unconstrained optimization function `fminunc` (exploiting quasi-Newton method) minimizing the following cost function,

$$\beta = \|\mathbf{e}(t_f)\|^2 + \|\boldsymbol{\zeta}(t_f)\|^2 + H(t_f)^2 \tag{45}$$

while varying the 21 varied parameters, $\mathbf{X} = [\lambda_1(t_0), \ldots, \lambda_{20}(t_0), t_f]^T$. By default, the termination tolerance for the function value and on vector of varied parameters was set to 10^{-6}.

For the case of path constraints placed on the state variables as in Eq. (30), 20 additional parameters were added to define the costates values at the time, t_d, where they become discontinuous [12]. For this case a reset is included, along with the integrator that resets the costates to these new parameters if the path constraint is encountered. In this case, the **X** value is augmented to include initial guesses of the costate values for the time t_d [14]:

$$\mathbf{X} = [\lambda_1(t_0), \ldots, \lambda_{20}(t_0), \lambda_1(t_d), \ldots, \lambda_{20}(t_d), t_f]^T \tag{46}$$

The vector **X** is only augmented with enough costate reset values as suspected path constraint contact points deduced from the PSM solution. For example, the PSM solution suggests only one contact with the path constraint, therefore the **X** vector was augmented with only one set of $\lambda(t_d)$ values.

To implement the state path constraint of the form $h(\mathbf{x}) \geq 0$, where h does not depend on **u**, a penalty function **P** was associated with the violation of the constraint that took the form of

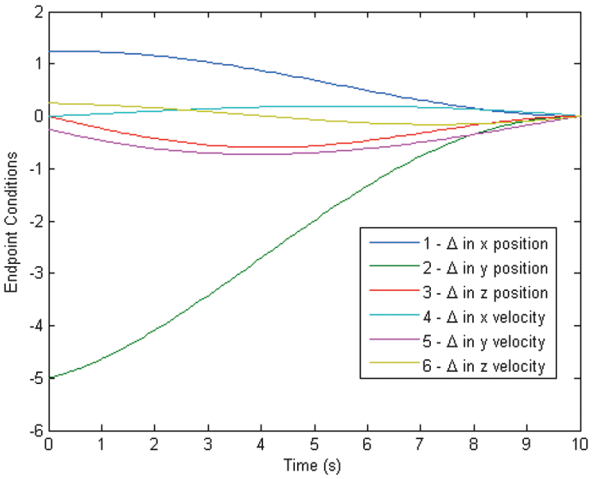

Fig. 5 Time history of discrepancies in the position and velocity of the chase and RSO docking points.

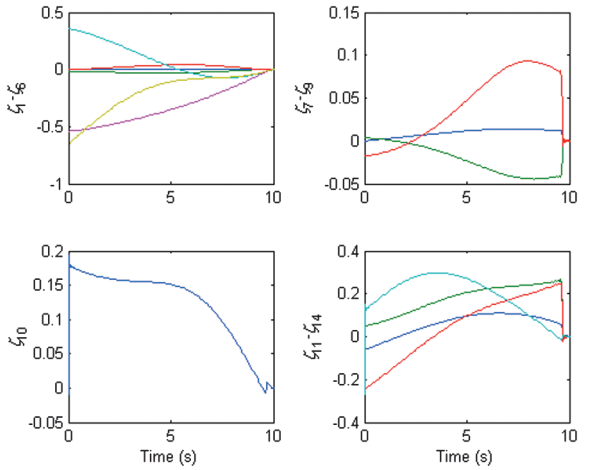

Fig. 6 Time history of discrepancies in the terminal conditions derived from transversality conditions.

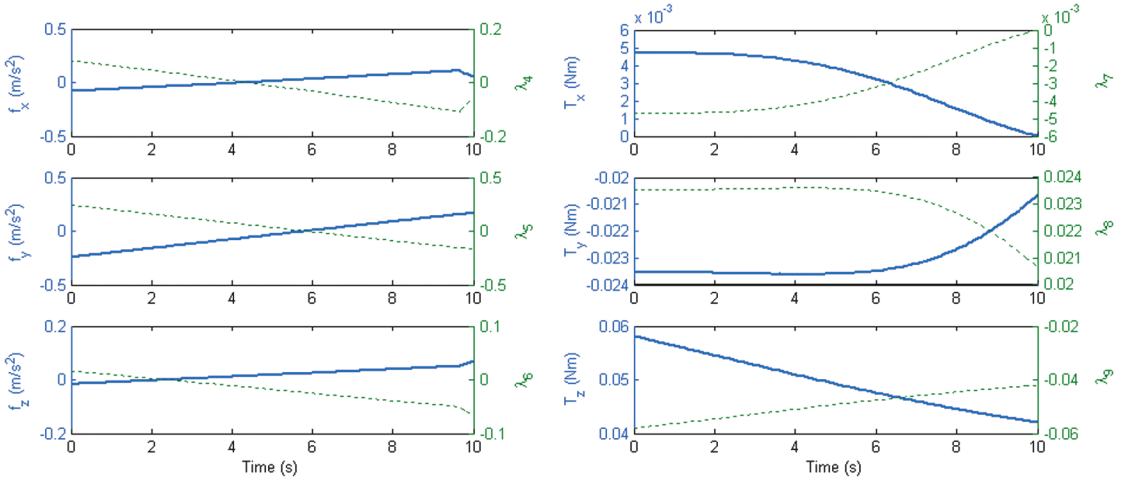

Fig. 4 Control and associated costate history resulting from the pseudospectral solution.

Table 2 Initial values of costates and t_f as defined by the pseudospectral solver

Variable	Initial condition	Variable	Initial condition	Variable	Initial condition
λ_1	0.0202713560903818	λ_8	0.0235328656506421	λ_{15}	−0.00357471284206
λ_2	0.0415555942048028	λ_9	−0.058080907113755	λ_{16}	1.060304309630e − 10
λ_3	0.00694445082087804	λ_{10}	−0.358237973748141	λ_{17}	−0.0681335012622741
λ_4	0.0816306658067988	λ_{11}	0.556788661928892	λ_{18}	0.0053037488085563
λ_5	0.244702539834469	λ_{12}	0.410549229662363	λ_{19}	0.202974770150912
λ_6	0.0166838774111	λ_{13}	1.41849853483e − 05	λ_{20}	−3.422927080667e − 10
λ_7	−0.004695462475917	λ_{14}	−2.046214161772e − 05	t_f	10

Table 3 Value of terminal and transversality conditions at the final time

Variable	Resulting value	Variable	Resulting value	Variable	Resulting value
$e_1(t_f)$	2.1e − 10	$\zeta_2(t_f)$	−9.9e − 09	$\zeta_9(t_f)$	7.7e − 08
$e_2(t_f)$	−9.4e − 12	$\zeta_3(t_f)$	−1.6e − 09	$\zeta_{10}(t_f)$	5.0e − 08
$e_3(t_f)$	−2.8e − 11	$\zeta_4(t_f)$	1.2e − 11	$\zeta_{11}(t_f)$	1.4e − 07
$e_4(t_f)$	5.1e − 11	$\zeta_5(t_f)$	−4.5e − 09	$\zeta_{12}(t_f)$	6.5e − 08
$e_5(t_f)$	1.7e − 10	$\zeta_6(t_f)$	2.6e − 09	$\zeta_{13}(t_f)$	3.3e − 07
$e_6(t_f)$	1.4e − 10	$\zeta_7(t_f)$	6.4e − 07	$\zeta_{14}(t_f)$	−5.8e − 07
$\zeta_1(t_f)$	3.8e − 07	$\zeta_8(t_f)$	−6.4e − 09	$H(t_f)$	−0.009711

$$\rho = \begin{cases} 2x_1x_4 + 2x_2x_5 + 2x_3x_6, & h \le 0 \\ 0, & h > 0 \end{cases} \tag{47}$$

with

$$P = \int_{t_0}^{t_f} \rho \, \mathrm{d}t \tag{48}$$

and

$$\beta = \|e(t_f)\| + \|\zeta(t_f)\| + H(t_f)^2 + P \tag{49}$$

used instead of Eq. (45). This takes care of increasing the cost function if the vehicle is on the constraint boundary and not meeting the tangency conditions stated in Sec. III.B. Otherwise, if the vehicle is not on the constraint or meets the tangency conditions while on the constraint, there will be no penalty associated with the cost. A penalty function of this type is also appealing because it has a smooth transition from solutions where constraints are not violated to

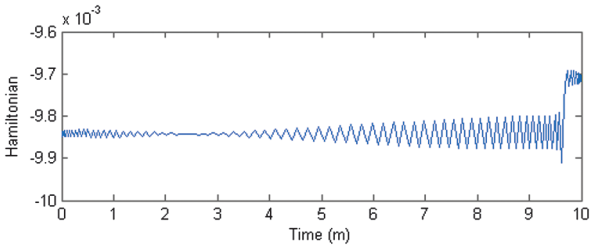

Fig. 7 Hamiltonian for the pseudospectral minimum-control solution.

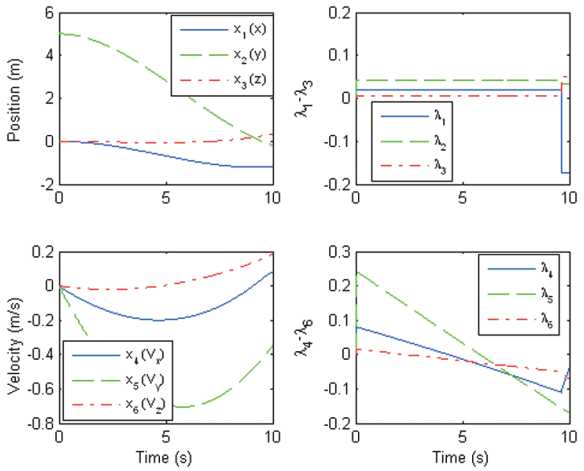

Fig. 9 State and costate time histories for chaser vehicle (MP solution).

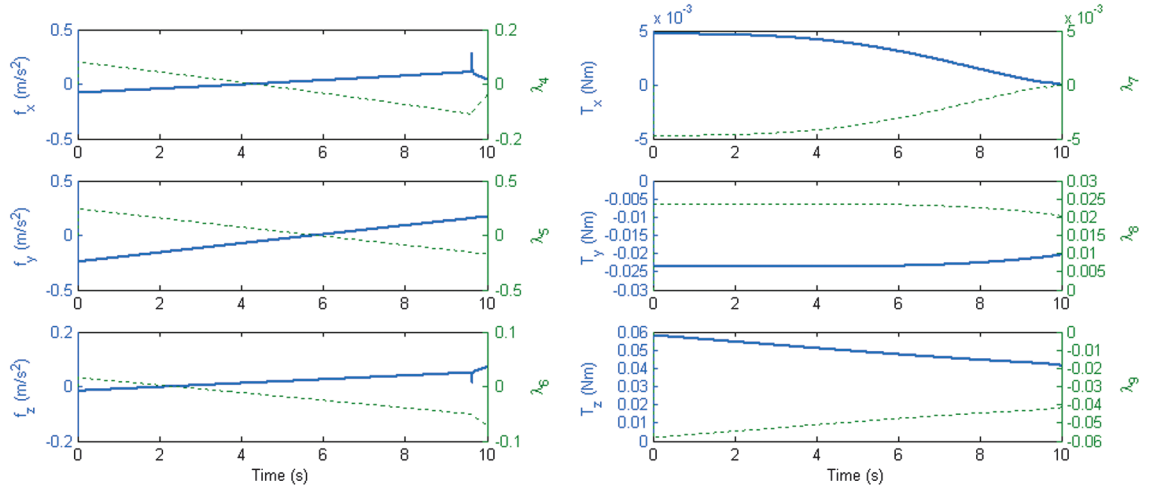

Fig. 8 Control time histories for the MP solution.

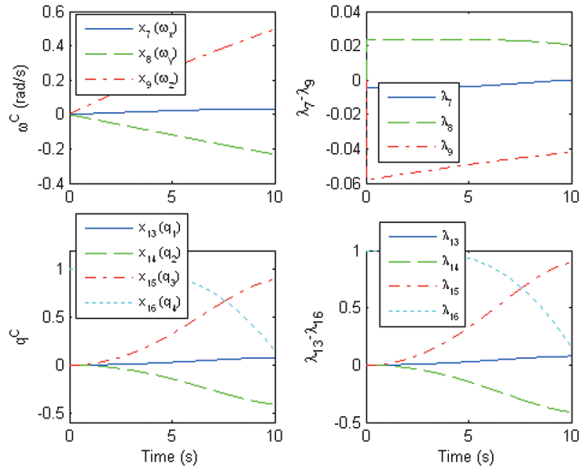

Fig. 10 State and costate histories for the defining angular parameters of the chaser vehicle (MP solution).

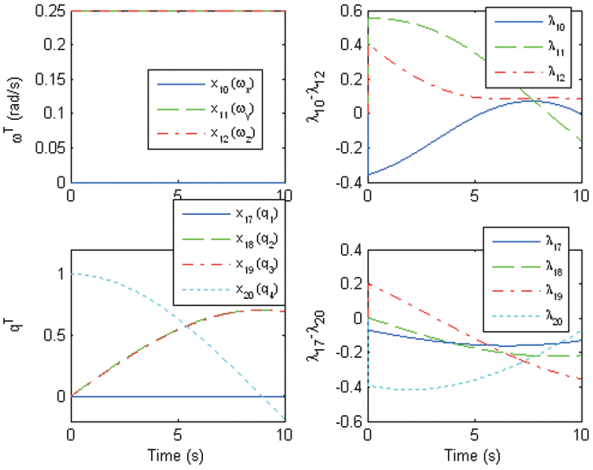

Fig. 11 State and costate time histories for the target vehicle (MP solution).

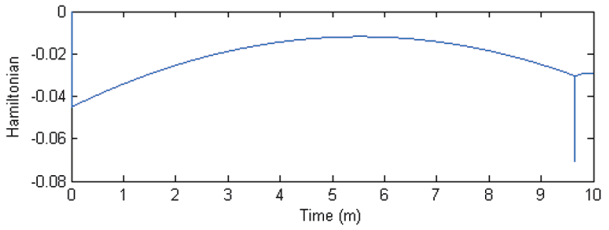

Fig. 12 Hamiltonian for the forward-shooting minimum-control solution.

solutions where they are violated. Note that if the vehicle is on the boundary and meets the tangency conditions, it will not cross the boundary.

V. Obtaining and Analyzing the Minimum-Control Solution

The minimum-control solution with the optimal controls defined in Eq. (14) is here presented first. First, the PSM solution is introduced and then its verification with the MP solution is discussed.

A. Minimum-Control Solution with the Pseudospectral Solver

For the minimum-control rendezvous scenario set in Sec. IV.A the pseudospectral method yielded the solution shown in Fig. 2. This solution returned a value of $J = 0.1133$ s. The overlaid sphere is centered on the target RSO and has a radius equal to that of the distance by which the docking point of the RSO is offset from its center of mass. Figure 3 shows the planar views of the solution. The final maneuver time is calculated to be 10 s, which is the upper bound on the final allowable time for this scenario (without this limit the optimal solution would yield an infinite final time).

Figure 4 shows a plot of the resulting controls histories (solid lines) as well as the associated costate histories (without units) that were used to synthesize the optimal control based on Eq. (14) (dashed lines). Figures 5 and 6 show the time histories of the vectors $\mathbf{e}(t)$ and $\boldsymbol{\zeta}(t)$, illustrating that all components approach zero at the end. Table 2 summarizes the results of optimization in terms of the values of varied parameters, initial value of the costates and Table 3 lists the terminal values of $\mathbf{e}(t)$, $\boldsymbol{\zeta}(t)$, and $H(t)$. Since the final value of the Hamiltonian does not tell a full story for numerical solutions, its complete time history is presented in Fig. 7.

Table 4 Initial values of costates and t_f as defined by MP

Variable	Initial condition	Variable	Initial condition	Variable	Initial condition
λ_1	0.0202713560903818	λ_8	0.0235328656506421	λ_{15}	−0.00357471284206**443**
λ_2	0.0415555942048028	λ_9	−0.058080907113755	λ_{16}	−0.**19**
λ_3	0.00694445082087804	λ_{10}	−0.358237973748141	λ_{17}	−0.0681335012622741
λ_4	0.0816306658067988	λ_{11}	0.556788661928892	λ_{18}	0.0053037488085563
λ_5	0.244702539834469	λ_{12}	0.410549229662363	λ_{19}	0.202974770150912
λ_6	0.0166838774111485	λ_{13}	−**3.08464082774455**e − 05	λ_{20}	−0.**39**
λ_7	−0.00469546247591**737**	λ_{14}	−2.**10412301393841**e − 05	t_f	10

Table 5 Value of terminal and transversality conditions at the final time

Variable	Resulting value	Variable	Resulting value	Variable	Resulting value
$e_1(t_f)$	0.0001	$\zeta_2(t_f)$	0.0001	$\zeta_9(t_f)$	0.0001
$e_2(t_f)$	−0.0001	$\zeta_3(t_f)$	−0.0001	$\zeta_{10}(t_f)$	−0.0001
$e_3(t_f)$	−0.0006	$\zeta_4(t_f)$	−0.0006	$\zeta_{11}(t_f)$	−0.0006
$e_4(t_f)$	−0.0033	$\zeta_5(t_f)$	−0.0033	$\zeta_{12}(t_f)$	−0.0033
$e_5(t_f)$	0.0012	$\zeta_6(t_f)$	0.0012	$\zeta_{13}(t_f)$	0.0012
$e_6(t_f)$	0.0013	$\zeta_7(t_f)$	0.0013	$\zeta_{14}(t_f)$	0.0013
$\zeta_1(t_f)$	−0.0001	$\zeta_8(t_f)$	−0.0001	$H(t_f)$	−0.0291

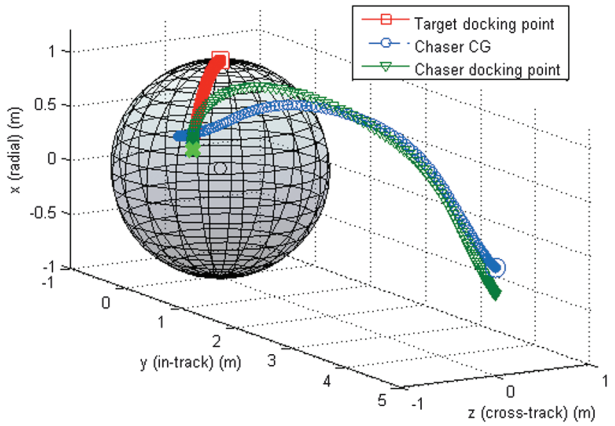

Fig. 13 Three-dimensional plot of minimum-time rendezvous trajectory (pseudospecral solver).

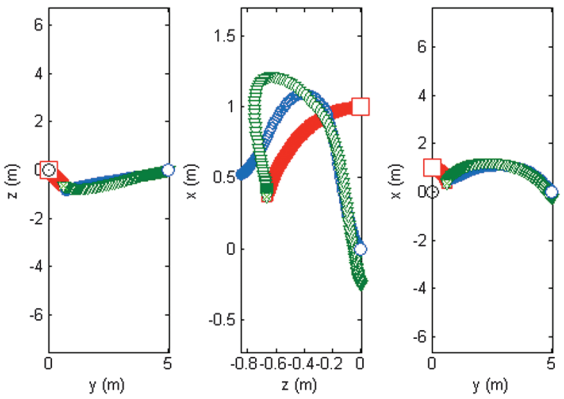

Fig. 14 Two-dimensional plots of minimum-time rendezvous trajectory (pseudospecral solver).

It should be noted that the achieved terminal tolerance of the order of 10^{-7}–10^{-11} does not necessarily indicate the quality of the solution. The reason for this is that the parameters of the trajectory are being computed (optimality conditions enforced) at only 150 nodes. Another important issue worth mentioning here is that it took 11,869.27 s (almost 3.3 h) to produce this 150-node solution of a 10-s-long trajectory on a 2.33 GHz Dell Precision M90 desktop computer with an Intel T7600 processor and 1 Gb of RAM. The initial guess for the solution (required as an input to the pseudospectral method) consisted of two terminal points, one at the initial time and one at the final time. The guess for the initial states corresponded to the initial conditions, and the guess for the final states consisted of zeros for the first 12 states and the value of $[0, 0, 0, 1]^T$ for the states corresponding to the quaternions. The guess for the control history was 0 at the initial and final times for all controls. A less accurate solution, with a lower number of nodes, would obviously require less computational resources [15]. For instance, a 25-node solution will require only 219.43 s (less than 4 minutes) on the same computer. The solution appears to be feasible and realizable in practice (as shown, in the smooth controls in Fig. 4), but can be used only for offline computations, i.e., in an open-loop guidance scheme. The jump in Hamiltonian value in Fig. 7 and other Hamiltonian histories to follow occurs when the path constraint from Eq. (30) is enforced as in Eq. ().

B. Verification of the Pseudospectral Solution with the Minimum Principle

As discussed in Sec. IV.C the initial guesses provided by the PSM solution (Table 2) were used to run an optimization procedure exploiting the optimal controls synthesized using the MP. The quasi-Newton-method-based optimization routine employing forward shooting and integration of equations of motion using a Bogacki–Shampine Rungei–Kutta method of order 3 [16] with a fixed step of 10^{-3}. This approach results in a solution that has as many as 10,000 points (as opposed to just 150 nodes as in the pseudospectral method). Of course, it comes with an increased computational cost. Even with the perfect initial guesses for all varied parameters it takes many hours or even days for the optimization process to converge (compared with the minutes or hours for the PSM). The MP solution, returned a value of the performance index $J = 0.11341185$ (compare with $J = 0.1133$ for the PSM solution), cost function $\beta = 0.001768$, and $P = 1.646\text{e} - 06$.

As expected, solving the same problem as in Sec. V.B (a quadratic control case with path constraints) produces the results, the optimal trajectory, controls, and time histories of all parameters, which are pretty close to those produced by the PSM. To save space here, we choose to present only control time histories and those states and costates that were not shown for the PSM solution. Specifically, Fig. 8 shows the control time histories, discontinuous when the path constraint is intersected at $t_d = 9.642$ s, and Figs. 9–11 show the states and corresponding costates of the chaser and target RSO. The values of the initial costates as suggested by the MP are shown in Table 4, and the terminal values $\mathbf{e}(t_f)$, $\boldsymbol{\zeta}(t_f)$, and $H(t_f)$ are shown in Table 5. Figure 12 presents the time history of the Hamiltonian.

Note that some of the values in Table 4 appear in the boldface. These are the only values that differ from the PSM solution (Table 2). Obviously, the numerical integration is quite sensitive to the initial values of the varied parameters. However, the results obtained by applying the minimum principle verify that the pseudospectral solver provides a solution very close to the truly optimal one.

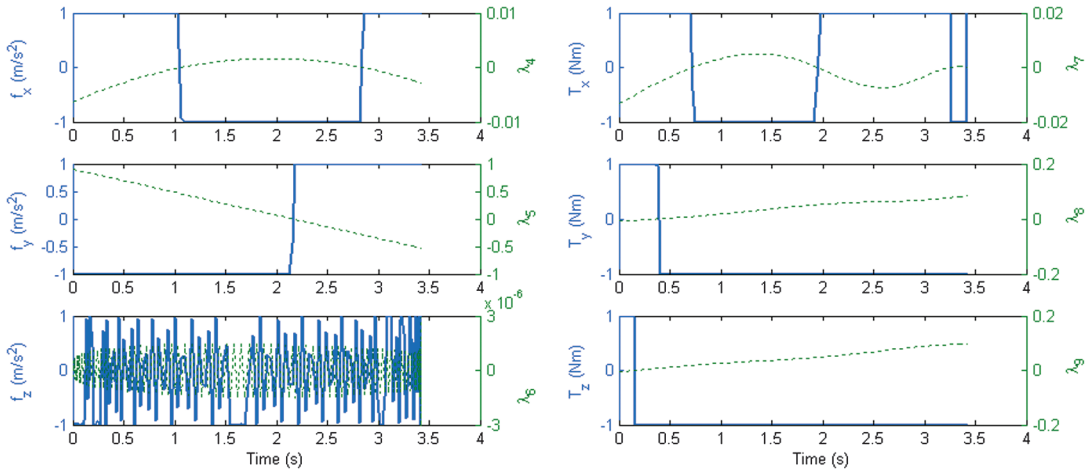

Fig. 15 Control and associated costate history resulting from the pseudospectral solver.

Table 6 Iinitial values of costates and t_f as defined by the PSM

Variable	Initial condition	Variable	Initial condition	Variable	Initial condition
Λ_1	0.000834092040702561	λ_8	−0.00781391345181247	λ_{15}	−0.0670307214682799
Λ_2	0.418560914087817	λ_9	−0.00529954719645793	λ_{16}	−2.47014407229089
Λ_3	7.46232139969827e − 08	λ_{10}	−0.0966015054618492	λ_{17}	−0.365359323439127
Λ_4	−0.00634589252204042	λ_{11}	0.017598938378927	λ_{18}	0.0400467496481145
Λ_5	0.901334242652277	λ_{12}	−0.719562963054045	λ_{19}	−0.562241844247041
Λ_6	1.04649495108653e − 07	λ_{13}	−0.0420682846405162	λ_{20}	−1.6978671241818
Λ_7	−0.0133948065189441	λ_{14}	−0.0394802339637517	t_f	3.4237

Table 7 Value of terminal conditions at the final time as calculated by the PSM

Variable	Resulting value	Variable	Resulting value	Variable	Resulting value
$e_1(t_f)$	−3.1e − 08	$\zeta_2(t_f)$	3.3e − 07	$\zeta_9(t_f)$	−1.9e − 06
$e_2(t_f)$	−3.8e − 08	$\zeta_3(t_f)$	−6.9e − 08	$\zeta_{10}(t_f)$	3.8e − 06
$e_3(t_f)$	4.9e − 08	$\zeta_4(t_f)$	−5.2e − 14	$\zeta_{11}(t_f)$	3.2e − 07
$e_4(t_f)$	−1.8e − 07	$\zeta_5(t_f)$	1.0e − 07	$\zeta_{12}(t_f)$	−5.1e − 07
$e_5(t_f)$	5.1e − 07	$\zeta_6(t_f)$	1.0e − 07	$\zeta_{13}(t_f)$	−2.0e − 07
$e_6(t_f)$	−1.7e − 08	$\zeta_7(t_f)$	−3.5e − 07	$\zeta_{14}(t_f)$	1.1e − 07
$\zeta_1(t_f)$	−3.3e − 10	$\zeta_8(t_f)$	9.7e − 06	$H(t_f)$	−0.2801

VI. Obtaining and Analyzing the Minimum-Time Solution

A. Minimum-Time Solution with the PSM

The three-dimensional trajectory and two-dimensional projections of the trajectories given by the pseudospectral solver are shown in Figs. 13 and 14, respectively. Evidently, they are different from those shown in Figs. 2 and 3. The resulting control history is shown in Fig. 15. The f_z control (of the translational motion in the z direction) turns out to be highly oscillating. The values of the initial costates as suggested by the PSM are shown in Table 6 and the terminal conditions of the boundary equations are shown in Table 7. The time history for the Hamiltonian is presented in Fig. 16.

Closer inspection of the pseudospectral solution for λ_6 in Fig. 15 (it jumps around zero value) suggests the presence of a singular control. This is indirectly confirmed by oscillations of the Hamiltonian. Hence, the f_z control is not only not optimal, it is infeasible as well.

With 150 nodes the computational time to arrive at the solution shown above (3.4237 s maneuver) was 8,929.55 s (∼2.5 h). (The initial guess for the solution was the same as the one used for the minimum-energy case.) For comparison, with 25 nodes the required computational time can be reduced to only 100.77 s (less than 2 min). However, as shown in Fig. 17 the controls in this case are even less optimal than in Fig. 15, and, of course, the Hamiltonian (Fig. 18) varies even more than that of Fig. 16.

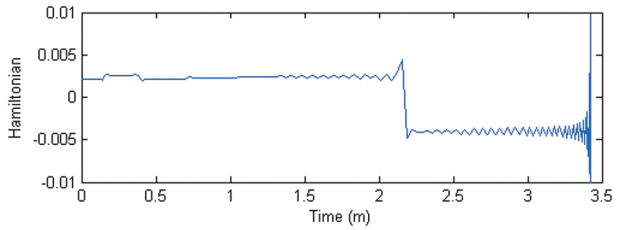

Fig. 16 Hamiltonian for the minimum-time solution (pseudospectral solver).

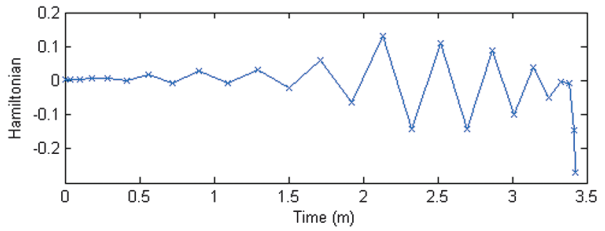

Fig. 18 Hamiltonian for the pseudospectral minimum-time 25-node solution.

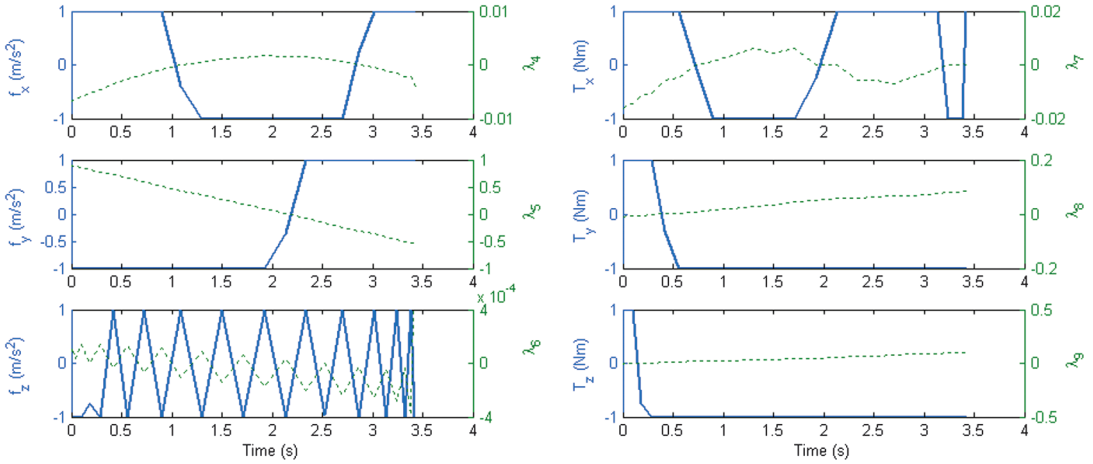

Fig. 17 Control and associated costate history resulting from the pseudospectral solution with 25 nodes.

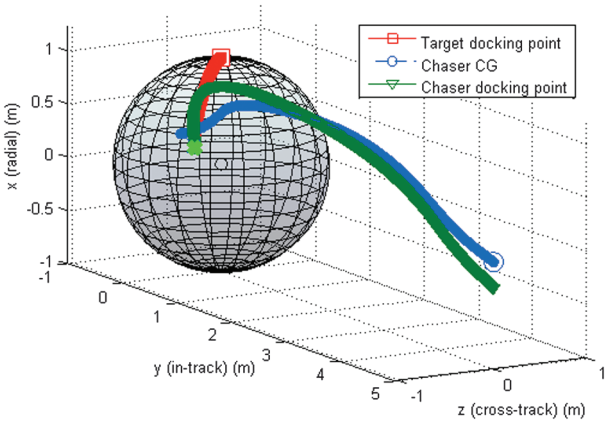

Fig. 19 Three-dimensional minimum-time rendezvous trajectory by MP.

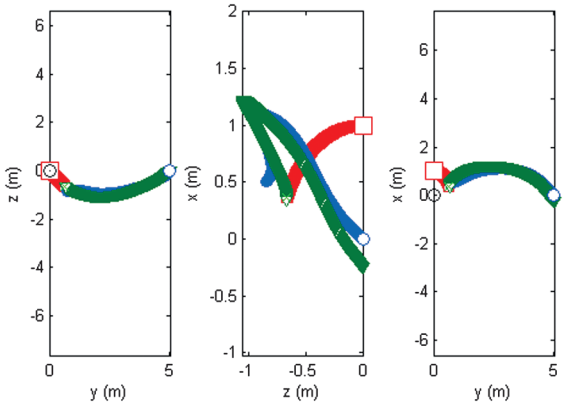

Fig. 20 Two-dimensional projections of minimum-time rendezvous trajectory.

B. Verification of the Pseudospectral Solution with the Minimum Principle

The minimum-time rendezvous problem is approached in a similar fashion to the minimum control. First, the problem is investigated using the cost function in Eq. (49). A major difference that arises compared with the minimum-control solution is the existence of a singular control in u_3, which controls acceleration in the z orbital direction. As discussed in Sec. III.C, the analytical synthesis of the singular control is quite bulky and therefore was not derived, but in the numerical solution it was handled as follows. The optimal control structure was assumed to have the following form:

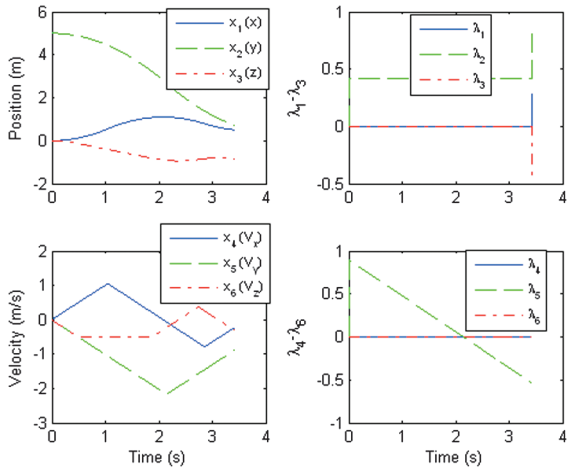

Fig. 22 State and costate histories for the chaser vehicle.

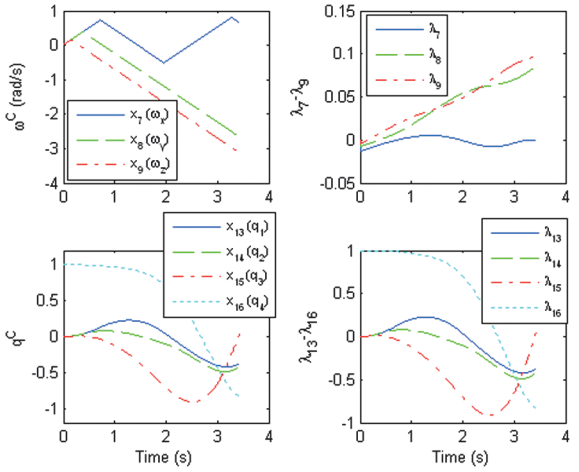

Fig. 23 State and costate histories for the defining angular parameters of the chaser vehicle.

$$u_3 = \begin{cases} -1, & 0 \le t < t_1 \\ 0, & t_1 \le t < t_2 \\ 1, & t_2 \le t < t_3 \\ 0, & t_3 \le t < t_4 \\ -1, & t_4 \le t < t_5 \\ 0, & t_5 \le t < t_6 \\ 1, & t_6 \le t < t_f \end{cases} \tag{50}$$

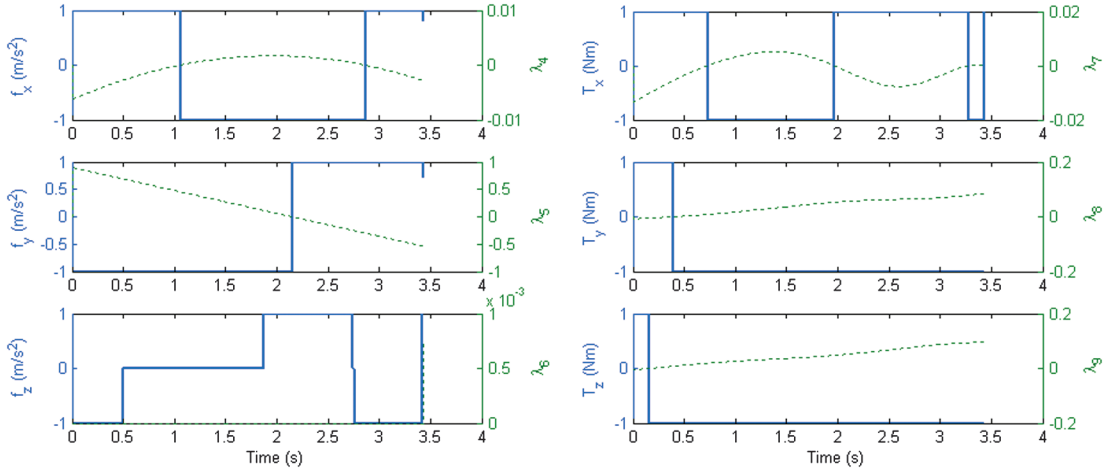

Fig. 21 Minimum-time rendezvous control histories by MP.

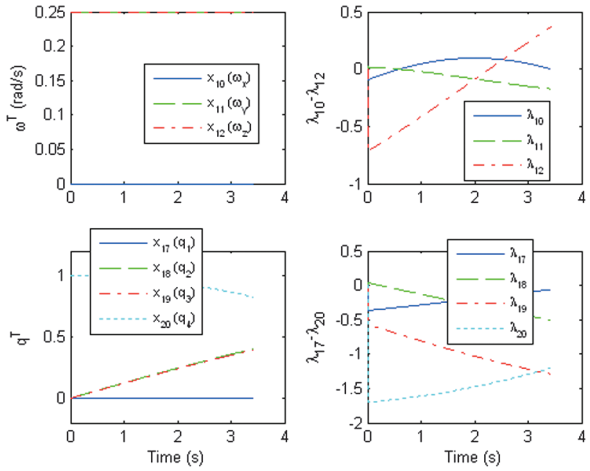

Fig. 24 State and costate time histories for the target vehicle.

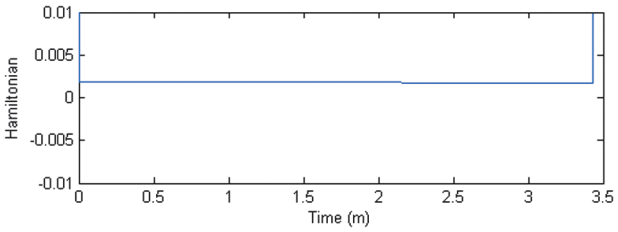

Fig. 25 Hamiltonian for the forward-shooting minimum-time solution.

Accordingly, the vector of varied parameters $\mathbf{X}$ was augmented with the switching times $t_1, \ldots, t_6$

$$\mathbf{X} = [\lambda_1(t_f), \ldots, \lambda_{20}(t_f), \lambda_1(t_d), \ldots, \lambda_{20}(t_d), t_1, \ldots, t_6, t_f]^T \quad (51)$$

Having instances $t_1, \ldots, t_6$ as varied parameters implied that the search was made among multiple control profiles including traditional bang–bang control, such as $u_{3\min} - u_{3\max}$ (when $t_1 = t_2$ and $t_i = t_f$ for $i = 3, \ldots, 6$), or $u_{3\max} - u_{3\min}$ (when $t_1 = t_2 = 0$, $t_3 = t_4$, and $t_5 = t_6 = t_f$ for $i = 3, \ldots, 6$) and bang–off–bang control.

The resulting trajectory is shown in Figs. 19 and 20. The corresponding optimal controls profiles are presented in Fig. 21. As shown, the $u_{3\min} - 0 - u_{3\max} - u_{3\min}$ profile was found to be optimal for the u_3 control (i.e., $t_5 = t_6 = t_f$). The time histories for the remaining controls (u_1, u_2, u_4, u_5, and u_6) match those for the pseudospectral solution (Fig. 12). Figures 22–24 show the states and costates time histories for the chaser and target RSO, respectively. The values of the initial costates as determined by the MP are shown in Table 8 and the errors in satisfying boundary conditions are shown in Table 9. It results $\beta = 0.002$ and $P = 0.00124$. Figure 25 presents the Hamiltonian (cf. Figs. 16 and 18).

Again, the boldface values in Table 8 indicate the differences as compared with the pseudospectral quasi-optimal solution. As opposed to the minimum-control case, when the truly optimal solution happened to have almost the same values of the initial costates, in the minimum-time case implying a singular control, the optimal solution involved more variations from the solution provided by the pseudospectral method. Of course, as in the minimum-control case presented in Sec. V, the indirect-method-based optimization was run recursively multiple times for several days in order to converge. Nevertheless, the errors in satisfying the terminal conditions (Table 9) were of several orders higher than those of claimed by the pseudospectral solution (Table 7). The next section provides some more details on this issue.

C. Propagation of the Pseudospectral Solution

Once again, for the solutions provided by the pseudospectral solver, vehicle dynamics are satisfied only at a limited number of nodes. That is why the error in meeting all constraints is so negligibly small as compared with solutions provided by the methods involving integration of equations of motion (shooting method). However, if the controls given by the pseudospectral solver are used as forcing functions, and the dynamics are numerically integrated, the resulting accuracy is similar to the one obtained by the shooting approach.

To illustrate this, consider the example of the controls for the minimum-time solution (including an arbitrary control for f_z) and integrate it. The result of integrating the equations of motion derived in Secs. II and III with a fixed time step of 0.0001 s is shown in Figs. 26 and 27 (the zeroth-order hold of the last control inputs was used). The trajectories are practically the same as in Figs. 13 and 14, but the endpoint discrepancies, summarized in Table 10, obviously grew. Figure 28 shows a progression of the chaser spacecraft as it approaches the orientation of the RSO at the final time. The endpoint conditions of the state variables are shown in Table 10. Note that the endpoint conditions of the transversality conditions are not known, because the costates are not propagated.

Table 8 Initial values of costates and t_f as defined by MP

Variable	Initial condition	Variable	Initial condition	Variable	Initial condition
λ_1	0.000813270815835508	λ_8	−0.007**90439447849 84**	λ_{15}	−0.067030**975848676**
λ_2	0.41856021740054	λ_9	−0.0052**514744594656**	λ_{16}	−2.4701**3927846309**
λ_3	0	λ_{10}	−0.0966015055**875181**	λ_{17}	−0.365359**450504476**
λ_4	−0.0063**2550328119496**	λ_{11}	0.017598938703864	λ_{18}	0.0400468901069352
λ_5	0.90134410424794	λ_{12}	−0.719562962**786195**	λ_{19}	−0.562241**768137901**
λ_6	0	λ_{13}	−0.0420**50296747438**	λ_{20}	−1.6978671241818
λ_7	−0.013**5549835134852**	λ_{14}	−0.039**5088309550527**	t_f	3.432

Table 9 Value of terminal and transversality conditions at the final time

Variable	Resulting value	Variable	Resulting value	Variable	Resulting value
$e_1(t_f)$	0.016	$\zeta_2(t_f)$	0.0028	$\zeta_9(t_f)$	0.0096
$e_2(t_f)$	−0.014	$\zeta_3(t_f)$	−0.0018	$\zeta_{10}(t_f)$	0.0061
$e_3(t_f)$	0.0016	$\zeta_4(t_f)$	0.00013	$\zeta_{11}(t_f)$	0.00048
$e_4(t_f)$	−0.017	$\zeta_5(t_f)$	−0.00059	$\zeta_{12}(t_f)$	−0.00079
$e_5(t_f)$	0.029	$\zeta_6(t_f)$	−0.00077	$\zeta_{13}(t_f)$	0.0010
$e_6(t_f)$	0.0080	$\zeta_7(t_f)$	0.0066	$\zeta_{14}(t_f)$	6.6e − 05
$\zeta_1(t_f)$	1.9e − 05	$\zeta_8(t_f)$	−0.0063	$H(t_f)$	0.15

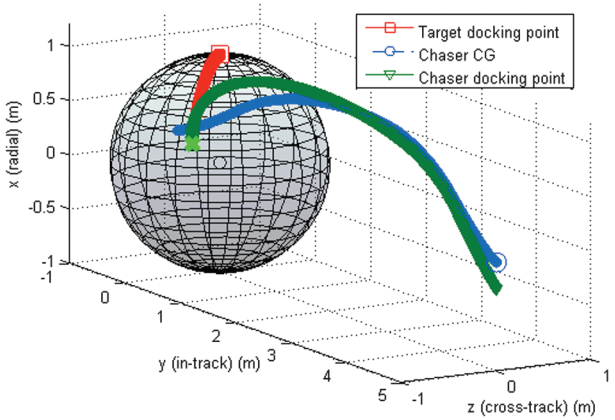

Fig. 26 Propagated trajectory using the minimum-time control history from the pseudospectral solver.

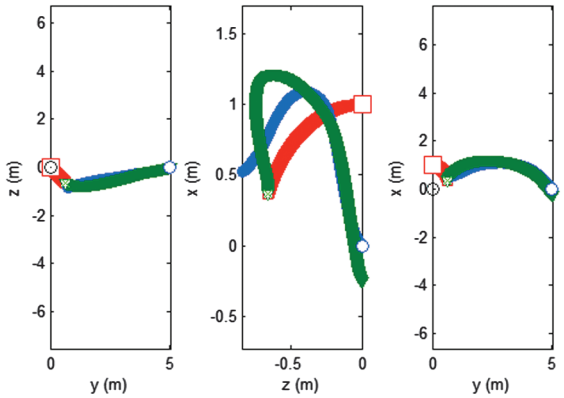

Fig. 27 Propagated trajectory using the minimum-time control history from the pseudospectral solver.

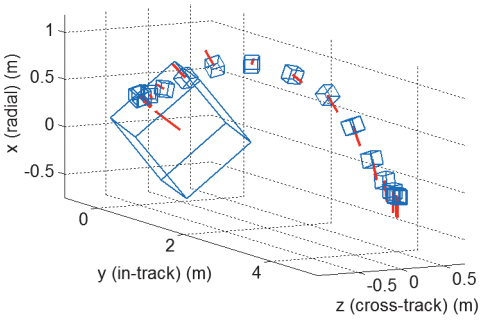

Fig. 28 Propagated trajectory using the minimum-time control history from the pseudospectral solver.

VII. Conclusions

The paper presented a six-degree-of-freedom 20-state model of a two-spacecraft rendezvous. The minimum-quadratic-control and minimum-time continuous-optimal-control problems were formulated and addressed using one of the direct collocation (pseudospectral) methods. For both problems, the desired optimal trajectory of chaser spacecraft with respect to a tumbling resident space object is sought such that the desired docking points match in position and velocity. Moreover, the solutions obtained were verified based on the minimum principle, numerically solved by using a shooting approach. That included derivation of the adjoint equations, formulation of the necessary conditions for the optimal solution, and synthesis of the optimal controls. The results obtained from using the direct method are very close to those obtained using the minimum principle. It was also found that path constraints are necessary when solving for the optimal trajectory in order to prevent undesired collision of the spacecraft. This was shown by the active path constraint that results in discontinuous costates upon contact with the constraint boundary.

As expected, the pseudospectral solver method was found to be reliable and yielded the results relatively fast. Moreover, these results were also validated via propagation of the states based on the system dynamics and previously calculated optimal controls. However, the pseudospectral method proved to be unable to produce the results fast enough so that it could be used in real time. Hence, in the near future it leaves only an offline open-loop option to be used on a real spacecraft. But even then, it was found that in the case of a singular control, the method returns somewhat infeasible results. That suggests avoiding using the time of maneuver as a performance index, but rather blend it with some other criterion such as control expenditure. The main simplifying hypothesis considered in the numerical simulation presented in the present paper was the spherical inertial symmetry of both chaser and target spacecraft as well as thrust control limits being applied in the orbital frame, regardless of chaser spacecraft orientation. To achieve feasible controls in real time, further study is required to remove this hypothesis, along with an investigation of the usage of different combined performance indexes and other direct methods such as one based on the inverse dynamics of the problem.

Acknowledgments

The authors thank James Riker, Chief Scientist of the U.S. Air Force Research Laboratory (AFRL) Space Vehicles Directorate, for his support of this project. The authors would also like to thank AFRL Space Vehicles Program managers William K. Schum and Lawrence Robbie Robertson.

References

[1] Davis, T. M., and Melanson, D., "XSS-10 Micro-Satellite Flight Demonstration Program," *Proceedings of the 17th Annual AIAA/USU Conference on Small Satellites*, Logan, UT, 11–14 Aug. 2003, pp. 99–99.

[2] Bosse, A. B., Barnds, W. J., Brown, M. A., Creamer, N. G. Feerst, A., Henshaw, C. G., et al., "SUMO: Spacecraft for the Universal Modification of Orbits," *Proceedings of SPIE: The International Society for Optical Engineering*, Vol. 5419, April 2004, pp. 36–46.

[3] David, L., "Military Micro-Sat Explores Space Inspection, Servicing Technologies," *Space.com*, www.space.com/businesstechnology/050722_XSS-11_test.html, Technology, 22 July 2005 [retrieved

Table 10 Value of terminal conditions at the final time

Variable	Resulting value	Variable	Resulting value	Variable	Resulting value
$e_1(t_f)$	−0.00027	$\zeta_2(t_f)$	N/A	$\zeta_9(t_f)$	N/A
$e_2(t_f)$	−9.3e − 05	$\zeta_3(t_f)$	N/A	$\zeta_{10}(t_f)$	N/A
$e_3(t_f)$	0.00037	$\zeta_4(t_f)$	N/A	$\zeta_{11}(t_f)$	N/A
$e_4(t_f)$	−0.00092	$\zeta_5(t_f)$	N/A	$\zeta_{12}(t_f)$	N/A
$e_5(t_f)$	−0.00035	$\zeta_6(t_f)$	N/A	$\zeta_{13}(t_f)$	N/A
$e_6(t_f)$	0.00026	$\zeta_7(t_f)$	N/A	$\zeta_{14}(t_f)$	N/A
$\zeta_1(t_f)$	N/A	$\zeta_8(t_f)$	N/A	$H(t_f)$	N/A

20 July 2009].
[4] Dornheim, M. A., "Orbital Express to Test Full Autonomy for On-Orbit Service," *Aviation Week & Space Technology*, www.aviationnow.com/avnow/news/channel_awst_story.jsp?id=news/aw060506p1.xml, 4 June 2006 [retrieved 20 July 2009].
[5] Friend, R. B., "Orbital Express Program Summary and Mission Overview," *Proceedings of SPIE: The International Society for Optical Engineering*, Vol. 6958, 2008, Paper 695803. doi:10.1117/12.783792
[6] Ma, Z., Ma, O., and Shashikanth, N., "Optimal Approach to and Alignment with a Rotating Rigid Body for Capture," *Journal of the Astronautical Sciences*, Vol. 55, No. 4, 2007, pp. 407–409.
[7] Sakawa, Y., and Shindo, Y., "On Global Convergence of an Algorithm for Optimal Control," *IEEE Transactions on Automatic Control*, Vol. 25, No. 6, 1980, pp. 1149–1153. doi:10.1109/TAC.1980.1102517
[8] Boyarko, G., Yakimenko, O., and Romano, M., "Optimization of a Spacecraft Maneuver to Dock with a Tumbling Object," AAS/AIAA Astrodynamics Specialist Conference, Pittsburgh, PA, American Astronautical Society, Paper AAS-09-316, 9–13 Aug. 2009.
[9] Vallado, D. A., and McClain, W. D., *Fundamentals of Astrodynamics and Applications*, Microcosm Press/Springer, New York, 2007, pp 374–379.
[10] Greenwood, D. T., *Principles of Dynamics*, Prentice–Hall, Upper Saddle River, NJ, 1987, pp. 392–393.
[11] Wie, B., *Space Vehicle Dynamics and Control*, AIAA Education Series, AIAA, Reston, VA, 1998.
[12] Kirk, D. E., *Optimal Control Theory: An Introduction*, Dover, New York, 2004, pp. 195–196.
[13] Bryson, A. E., Jr., and Ho, Y.-C., *Applied Optimal Control: Optimization, Estimation, and Control*, Taylor and Francis, New York, 1975, pp. 117–119.
[14] Rao, A. V., Benson, D. A., Darby, C. L., Patterson, M. A., Francolin, C., Sanders, I., and Huntington, G. T., "GPOPS: A MATLAB Software for Solving Multiple-Phase Optimal Control Problems Using the Gauss Pseudospectral Method," *ACM Transactions on Mathematical Software*, Vol. 37, No. 2, 2010, Paper 22. doi:10.1145/1731022.1731032
[15] Yakimenko, O., Xu, Y., and Basset, G., "Computing Short-Time Aircraft Maneuvers Using Direct Methods," AIAA Guidance, Navigation and Control Conference and Exhibit, AIAA Paper 2008-6632, Honolulu, HI, 18–21 Aug. 2008.
[16] Bogacki, P., and Shampine, L. F., "A 3(2) Pair of Rungei–Kutta Formulas," *Applied Mathematics Letters*, Vol. 2, No. 4, 1989, pp. 321–325. doi:10.1016/0893-9659(89)90079-7